Aerosol and Air Quality Research, 15: 1–10, 2015

ISSN: 1680-8584 print / 2071-1409 online
doi: 10.4209/aaqr.2014.10.0246

A Concept of a Novel Solar-Assisted Large-Scale Cleaning System (SALSCS) for Urban Air Remediation

Qingfeng Cao[1], David Y.H. Pui[1,2*], Wojciech Lipiński[3†]

[1] *Department of Mechanical Engineering, University of Minnesota, 111 Church Street SE, Minneapolis, Minnesota 55455, USA*
[2] *Faculty of Science, The University of Hong Kong, Hong Kong*
[3] *Research School of Engineering, The Australian National University, Canberra, ACT 0200, Australia*

ABSTRACT

A solar-assisted large-scale cleaning system (SALSCS) is proposed for air pollution abatement. The system consists of a large-scale flat-plate solar collector, a chimney, and a filter bank. In the basic configuration, an air flow is driven exclusively by buoyancy generated in the collector–chimney system, and $PM_{2.5}$ and larger particulate matter is separated from the air in the filter bank. The proof of concept is obtained by means of a transient 3D numerical simulation of fluid and heat flow for a full-scale system, implemented in ANSYS Fluent and performed using high-performance computing techniques. The effects of the filter bank on the system performance including heat transfer and fluid flow characteristics are evaluated by studying two system configurations, without and with a filter bank, respectively. The proposed SALSCS system is predicted to be capable of processing atmospheric air at a flow rate of 2.64×10^5 m^3/s, corresponding to the volume of 22.4 km^3 of polluted air remediated in 24 hours.

Keywords: SALSCS; Air remediation; $PM_{2.5}$ pollution; Solar; Numerical simulation.

INTRODUCTION

Effective approaches to abatement of air pollution are required in the context of the world-wide growth of particulate matter emissions from mobile and stationary sources such as transportation and industrial processing for energy conversion and extraction of natural resources. Many large urban areas experience unacceptably high local concentration of particulates, resulting in health hazards and lower living standards (Monks *et al.*, 2009). The United States Environmental Protection Agency (USEPA) established $PM_{2.5}$ standards for particulate matter (PM) in air of less than 2.5 μm in aerodynamic diameter. In January 2013, $PM_{2.5}$ was measured to be around 500–800 $\mu g/m^3$ in Beijing (Pui *et al.*, 2014). Between 2008 and 2011, the daily average of $PM_{2.5}$ in Delhi was 123 ± 87 $\mu g/m^3$ (Guttikunda and Calori, 2013). The concentrations at both locations significantly exceed the USEPA standards of 35 $\mu g/m^3$ and 12 $\mu g/m^3$ for daily and annual averages, respectively (Pui *et al.*, 2014). Air pollution has been shown to severely affect human health through respiratory and cardiovascular diseases, which leads to increased mortality rate (Seaton *et al.*, 1995; Bernstein *et al.*, 2004; Pöschl, 2005; Pope III and Dockery, 2006; Miller *et al.*, 2007; Pope III *et al.*, 2009; Chen *et al.*, 2013; Shah *et al.*, 2013; Pui *et al.*, 2014). Exposure to finer particle fractions such as $PM_{2.5}$ has a more pronounced effect on health deterioration than to coarser fractions such as PM_{10} (Schwartz *et al.*, 1996; Cifuentes *et al.*, 2000). Furthermore, the presence of particulate matter in the atmospheric air has been shown to impact the local and global climate through dimming, retarding monsoon circulation, changing the hydrological cycle and reduction of local precipitation (Ramanathan and Feng, 2009; Pöschl, 2005).

The idea of creating an air draft by solar heating is implemented in solar chimney power plants (Schlaich *et al.*, 2005; Zhou *et al.*, 2010; Dhahri and Omri, 2013). The first solar chimney power plant in the world was commissioned in Manzanares, Spain, in 1983 (Haaf *et al.*, 1983, 1984). Laboratory-scale prototypes (Pasumarthi and Sherif, 1998b; Zhou *et al.*, 2007) and new designs (Bilgen and Rheault, 2005; Cao *et al.*, 2011; Panse *et al.*, 2011) were developed in follow-up studies. Besides experimental investigations, mathematical and numerical models have been employed to evaluate plant performance. Pasumarthi and Sherif (1998a) developed a mathematical model to obtain a relationship

* Corresponding author.
Tel.: 1-612-625-2537; Fax: 1-612-625-6069
E-mail address: dyhpui@umn.edu
† Corresponding author.
Tel.: 61-2-612-57896
E-mail address: wojciech.lipinski@anu.edu.au

between the system parameters and its performance such as air temperature, velocity and power output. The model was validated using the experimental results from the Manzanares system (Pasumarthi and Sherif, 1998b). Bernardes and Weinrebe (2003) used a mathematical model to study the effects of geometry and ambient conditions on the power output of solar chimney power plants. Zhou *et al.* (2007) studied the effects of solar radiation intensity, solar collector area and chimney height on the system power output using a mathematical model validated using experimental results from their pilot prototype. Pastohr *et al.* (2004) conducted a 2D numerical simulation by solving the Reynolds-averaged Navier–Stokes equations (RANS) with a standard k–ε turbulence model. A theoretical analysis, validated using a numerical simulation, was carried out by Ming *et al.* (2006) to evaluate the performance of a solar chimney power plant. Numerical models were also used to study the effects of energy storage layer in the ground (Ming *et al.*, 2008a), rotation speed of the turbine (Ming *et al.*, 2008b), a strong ambient crosswind (Ming *et al.*, 2012) and chimney configurations (Ming *et al.*, 2013) on heat transfer and air flow and system power output. Sangi *et al.* (2011) developed both a mathematical model and a numerical model to conduct a detailed 2D analysis on the relationship between the solar radiation and the temperature, pressure and velocity profiles in the solar collector. Simulation results from the two models agreed well with the experimental data of the Manzanares prototype. A 3D numerical model developed by Guo *et al.* (2014) combined the radiation, solar load and turbine models to investigate the effects of different parameters including pressure drop across the turbine, solar radiation and ambient temperature, on the system performance. Fasel *et al.* (2013) conducted numerical simulations with ANSYS Fluent to verify analytical scaling laws, and obtained high-resolution time-dependent numerical results for a solar chimney power plant. High quality flow visualization was presented and flow instabilities were predicted.

Motivated by the developments of the solar chimney technology for power generation, we propose a solar-assisted large-scale cleaning system (SALSCS). This novel system consists of a large solar collector, a chimney and a filter bank and aims at generating air flows in large quantities to facilitate separation of particulate matter from polluted atmospheric air of urban areas. In this paper, a detailed system configuration is presented for an initial design. Heat and fluid flows are analyzed for the concept system using a transient 3D numerical model developed in ANSYS Fluent. Two configurations of the SALSCS, without and with a filter bank, are studied to evaluate its ability for generating air flow and the effect of the filter bank on the flow field.

SYSTEM DESCRIPTION

Fig. 1 shows a schematic diagram of the proposed SALSCS system. The system consists of a large glass collector (1), a chimney (2) and a filter bank (3). Buoyancy-

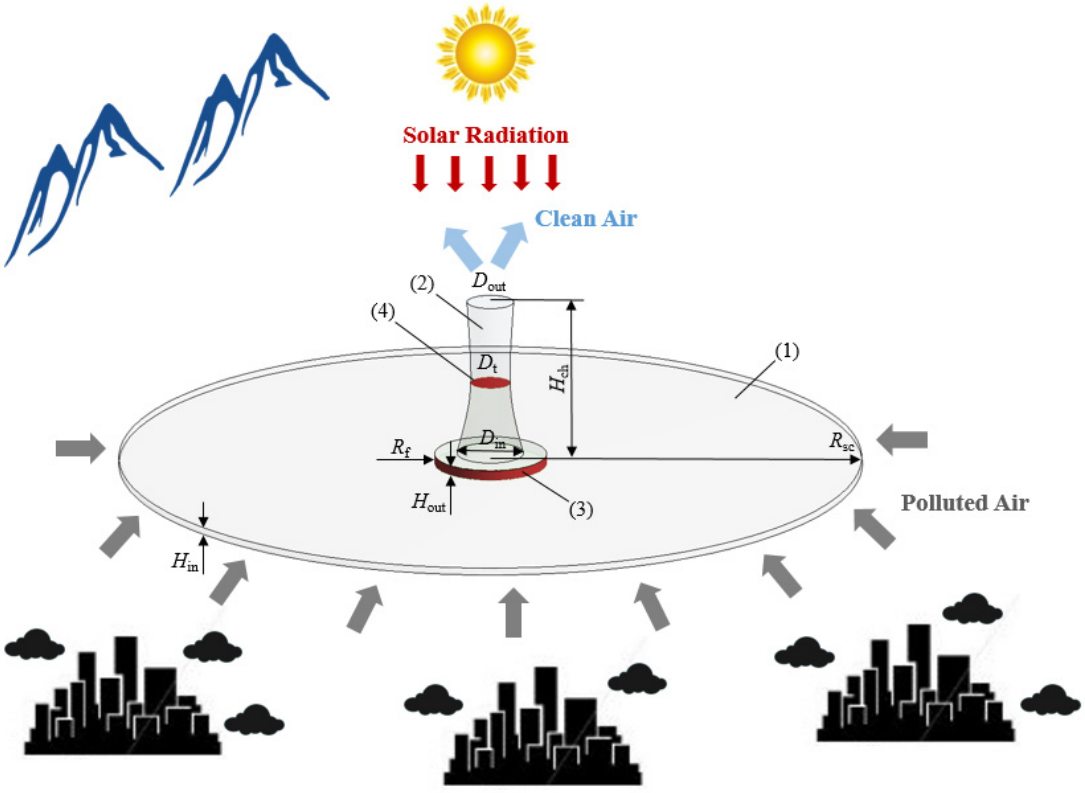

Fig. 1. Schematic diagram of the SALSCS system: (1) solar collector, (2) chimney, (3) filter bank, and (4) fan/turbine (optional).

driven flow is induced by solar heating of the collector. Atmospheric air enters the system at the aperture, passes through the collector while heated by contact with the ground and the cover glass plate, and further flows through the filter bank for separation of particulates. The filtered air enters the chimney and is drafted by buoyancy to the exit at the top. This chimney can be located either at the center of the collector or asymmetrically with respect to the collector. The filter bank can be built vertically in the collector along the circumference of the chimney base. To address solar intermittency, energy storage in soil or water under the collector can be employed. As an option, an air fan/turbine (4) can be installed inside the chimney to generate electricity during sunny days and induce air flow using grid-supplied electricity when solar radiation is not available for continuous 24-hour filtering.

To evaluate the ability of the SALSCS for air cleaning, a numerical simulation is conducted for a design with the chimney located at the center of the collector as depicted in Fig. 1. The shape of the chimney wall is given by two hyperbolas of revolution intersecting at the throat area of the chimney with the narrowest cross section. The chimney configuration has been adopted from the paper by Krätzig *et al.* (2011), which provides a detailed design to address flow instabilities and wind loads. In the baseline configuration, the height of the chimney measured with respect to the ground level is 500 m. The chimney diameter is 200 m at the base, 120 m at the throat and 136 m at its outlet. The collector occupies a circular area with a radius of 2500 m. Its height increases from 8 m to 20 m from the inlet to the bottom of the chimney supported by a circular plain area with a diameter of 332 m and uniform height of 20 m. The filter bank is located along the edge of this plain area. The main geometric parameters of the SALSCS system are listed in Table 1.

Table 1. Main geometric parameters of the SALSCS system.

Parameters	Value
R_{sc}	2500 m
H_{in}	8 m
H_{out}	20 m
H_{ch}	500 m
D_{in}	200 m
D_{out}	136 m
D_t	120 m
R_f	166 m

ANALYSIS

Since the geometry of the system configuration is axisymmetric, the 3D computational domain is reduced to a 45° segment of the full geometry with periodic boundary conditions applied at the two boundaries in the azimuthal direction (Fig. 2). To simulate the buoyancy-driven flow, the Boussinesq approximation is applied (Spiegel and Veronis, 1960). Rayleigh number is introduced to characterize the natural convection in the collector and the chimney,

$$\mathrm{Ra} = \frac{g\beta(T_{max} - T_{min})L^3}{\nu\alpha} \quad (1)$$

where g is the gravitational acceleration, β is the thermal expansion coefficient, L is the characteristic length taken equal to either the collector height or the chimney diameter, ν is the kinematic viscosity, α is the thermal diffusivity, and T_{max} and T_{min} are the maximum and minimum temperatures of the system, respectively. The resulting values of Rayleigh number are greater than 10^{10} for both the collector and the chimney, indicating that the air flow

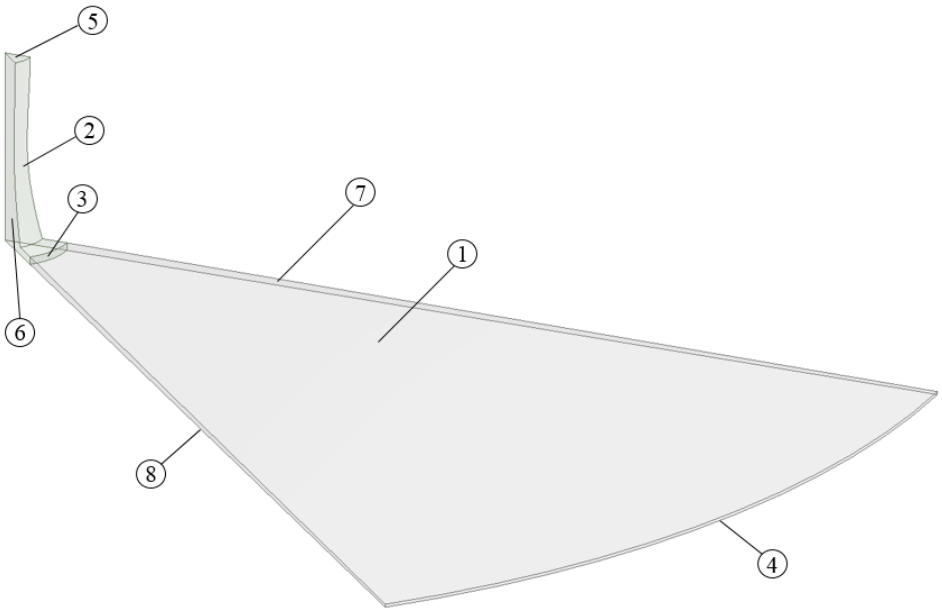

Fig. 2. Computation domain and boundaries. (1) Glass roof of the collector; (2) wall of the chimney; (3) filter bank; (4) inlet of the solar collector; (5) outlet of the chimney; (6) periodic boundary; (7) shadow of the periodic boundary; (8) ground surface.

in the SALSCS system is turbulent. The standard k–ε turbulent model available in ANSYS Fluent is chosen as an economic approach for complex turbulent flow modeling. Reynolds-averaged Navier–Stokes (RANS) equations are solved along with two additional transport equations for the turbulence kinetic energy (k) and turbulence kinetic energy dissipation rate (ε) (ANSYS, 2012).

Governing Equations

The numerical model is based on the continuity equation, the momentum equations for an incompressible flow with the additional buoyancy term, the energy equation, and the k–ε equations.

Continuity equation:

$$\frac{\partial u_i}{\partial x_i} = 0 \tag{2}$$

Momentum equations:

$$\rho\left(\frac{\partial u_i}{\partial t} + u_j\frac{\partial u_i}{\partial x_j}\right) = -\frac{\partial p}{\partial x_i} - \beta\rho(T - T_0)g_i + \mu\frac{\partial}{\partial x_j}\left(\frac{\partial u_i}{\partial x_j}\right) \tag{3}$$

Energy equation:

$$\frac{\partial T}{\partial t} + u_j\frac{\partial T}{\partial x_j} = \alpha\frac{\partial}{\partial x_j}\left(\frac{\partial T}{\partial x_j}\right) \tag{4}$$

Transport equation for the turbulent kinetic energy k:

$$\rho\frac{Dk}{Dt} = \frac{\partial}{\partial x_i}\left\{\left(\mu + \frac{\mu_t}{\sigma_k}\right)\frac{\partial k}{\partial x_i}\right\} + G_k + \beta g_j\frac{\mu_t}{\mathrm{Pr}_t}\frac{\partial T}{\partial x_j} - \rho\varepsilon \tag{5}$$

Transport equation for the energy dissipation rate ε:

$$\rho\frac{D\varepsilon}{Dt} = \frac{\partial}{\partial x_i}\left\{\left(\mu + \frac{\mu_t}{\sigma_\varepsilon}\right)\frac{\partial \varepsilon}{\partial x_i}\right\} + C_{1\varepsilon}\frac{\varepsilon}{k}\left(G_k + C_{3\varepsilon}\beta g_j\frac{\mu_t}{\mathrm{Pr}_t}\frac{\partial T}{\partial x_j}\right) - C_{2\varepsilon}\rho\frac{\varepsilon^2}{k} \tag{6}$$

In Eqs. (2–6), β and α are the air thermal expansion coefficient and thermal diffusivity, respectively. α is defined as $\alpha = K/\rho c_p$, where K is the thermal conductivity, ρ is the air density and c_p is the specific heat capacity at constant pressure. G_k represents the generation of turbulence kinetic energy caused by the mean velocity gradients,

$$G_k = -\rho\overline{u_i'u_j'}\left(\partial u_j / \partial u_i\right) \tag{7}$$

where $-\rho\overline{u_i'u_j'}$ are Reynolds stresses appearing in Reynolds-averaged Navier–Stokes (RANS) equations. The turbulent viscosity μ_t is given by

$$\mu_t = \frac{\rho C_\mu k^2}{\varepsilon} \tag{8}$$

where C_μ is a constant. Pr_t is the turbulent Prandtl number for energy and is modeled as a constant in the standard k–ε model in ANSYS Fluent. $C_{1\varepsilon}$, $C_{2\varepsilon}$ and $C_{3\varepsilon}$ are constants. σ_k and σ_ε are the turbulent Prandtl numbers for k and ε, respectively (ANSYS, 2012).

Boundary and Initial Conditions

The boundaries of the computation domain are shown in Fig. 2. The outer temperature at both the glass roof (1) and the inlet (4) of the solar collector is assumed equal to ambient temperature. Convection heat transfer occurs between the collector and the above ambient air as described by Eq. (9):

$$-K\left.\frac{\partial T}{\partial n_{sc}}\right|_{wall} = h\left(T - T_\infty\right) \tag{9}$$

where K is the thermal conductivity, n_{sc} is the local coordinate normal to the solar collector roof, and h is the convective heat transfer coefficient adopted from the study by Bernardes *et al.* (2007). The chimney wall (2) is assumed to be adiabatic as:

$$\left.\frac{\partial T}{\partial n_{ch}}\right|_{wall} = 0 \tag{10}$$

where n_{ch} is the local coordinate normal to the chimney wall. The fan boundary condition provided by ANSYS Fluent is utilized to simulate the pressure drop across the filter bank (3). The pressure drop typical of commercial large-scale filters varies from 200 Pa for a new filter to 800 Pa for a used filter (Donaldson, 2014). In this study, the pressure drop across the filter bank is assumed to be 498.3 Pa (which translates to 2 inches of water). The pressure at both the inlet (4) and outlet (5) of the system are set equal to the standard atmospheric pressure. In reality, the pressure at the chimney outlet (5) should be slightly lower than the pressure at the collector inlet (4) due to altitude difference. Periodic boundary conditions are applied at the two boundaries (6) and (7) in the azimuthal direction. For the boundary condition at the ground surface (8), a constant wall roughness is assumed. For simplicity, we apply a constant heat flux from the ground surface to the flowing air in the collector:

$$q'' = -K\left.\frac{\partial T}{\partial y}\right|_{y=0} \tag{11}$$

where q'' is the heat flux at the ground surface. The no-slip boundary condition is employed at all the wall-type boundaries of the computation domain. The initial conditions for the model can be expressed by Eqs. (12a) and (12b):

$$T\big|_{t=0} = 293.15K \tag{12a}$$

$$u_i\big|_{t=0} = 0 \quad (12b)$$

Numerical Solution

The finite volume method and the implicit Euler time integration scheme are employed to solve the governing equations as implemented in ANSYS Fluent. The pressure-based solver is used. SIMPLE algorithm is applied as the pressure-velocity coupling scheme, and PRESTO! algorithm is selected as the pressure interpolation scheme. The second order upwind scheme is chosen as the spatial discretization method for all governing equations. The numerical calculation is carried out with the double precision solver considering that our geometry has features of very disparate length scales. To monitor the solution convergence, the absolute convergence criterion of 10^{-8} is set for the energy equation and of 10^{-6} for all other equations. The time step size is set to be 0.005 s at the beginning and slightly increases to 0.05 s when the model shows a good convergence for each time step.

A hybrid meshing strategy is employed. Most of the computational domain is discretized with structured grids while unstructured grids are applied only in the inner region of the chimney and a part of the collector adjacent to the filter bank. 1,400,000+ cells are used in the numerical grid. To address the challenge of an excessive computational time associated with modeling the turbulent flow in the large geometry, parallel solution techniques with high-performance computing resources are employed. A simulation job requires 16 nodes each with 8 processor cores per node, and 2500 MB of RAM per processor core. Each node has two quad-core 2.8 GHz Intel Xeon X5560 "Nehalem EP"-class processors (Itasca, 2014).

RESULTS

Fluid flow and heat transfer are modeled for two configurations of SALSCS, without and with a filter bank, respectively, to evaluate its ability for generating air flow and identify the effect of the filter bank on the flow field. Air properties at the temperature of 20°C are used in the simulations and system input parameters for this study are listed in Table 2.

The gauge pressure contours on the computational domain boundaries of the two systems are shown in Fig. 3. A constant pressure drop of 498.3 Pa (2" H_2O) prescribed in the model along the filter bank is observed by comparing Figs. 3(a) and 3(b). According to the figures, the lowest gauge pressure appears near the bottom of the chimney, which equals to –920.4 Pa for the system without a filter bank and –931.5 Pa for the system including the filter bank. For both the two configurations, this low-pressure region results from vortices generated when the air enters the chimney with a relatively high velocity. The local pressure values along the centerlines of both the collector and the chimney are plotted in Figs. 4(a) and 4(b), respectively. Fig. 4(a) shows that the static pressure decreases from the inlet of the collector to the bottom of the chimney. There is also a pressure increase at the radial position from 100 m to 0 m resulting from air flow expansion at this location. Fig. 4(b) indicates the pressure profiles along the centerlines (y-axis) of the two systems' chimneys. The pressure in general increases back to the atmospheric pressure from the chimney bottom to the outlet. Obviously, a lower overall pressure drop in the system is obtained when the filter bank is not included in the system.

The velocity fields for the two SALSCS configurations are presented in Fig. 5. The highest velocity is found at the throat area of the chimney, 38.3 m/s and 26.3 m/s for the system without and with the filter bank, respectively. In addition, vortices appear near the low-pressure region at the bottom of the chimney as discussed before. The local velocity magnitudes along the centerlines of the collector and the chimney are plotted in Figs. 6(a) and 6(b), respectively. According to Fig. 6(a), the inlet velocity of the solar collector equals to 3.05 m/s for the system without a filter bank and 2.12 m/s as the filter bank is implemented. The velocity increases from the inlet to the outlet of the collector. At the radial position from 100 m to 0 m, it drops quickly, which is caused by the air flow expansion. Fig. 6(b) shows that the velocity magnitudes in the chimneys increases at first and decreases after the air passes through the throat of the

Table 2. Simulation input parameters.

Air Properties	Symbol	Value
Ambient air temperature	T_∞	293.15 K
Density	ρ	1.205 kg/m^3
Dynamic viscosity	μ	1.821×10^{-5} kg/m/s
Heat flux from the ground surface	q"	640 W/m^2
Heat transfer coefficient	h	8 W/m^2/K
Hydraulic diameter of the collector inlet	$D_{h,in}$	16 m
Inlet pressure of the collector	p_{in}	101325 Pa
Wall roughness at the ground surface	H_{wr}	0.05 m
Outlet pressure of the chimney	p_{out}	101325 Pa
Specific heat capacity	c_p	1005 J/kg/K
Thermal conductivity	K	0.0257 W/m/K
Thermal expansion coefficient	β	0.00343 K^{-1}
Turbulence intensity at the inlet	I_{in}	5%
Pressure drop across the filter bank	Δp	498.3 Pa (2" H_2O)

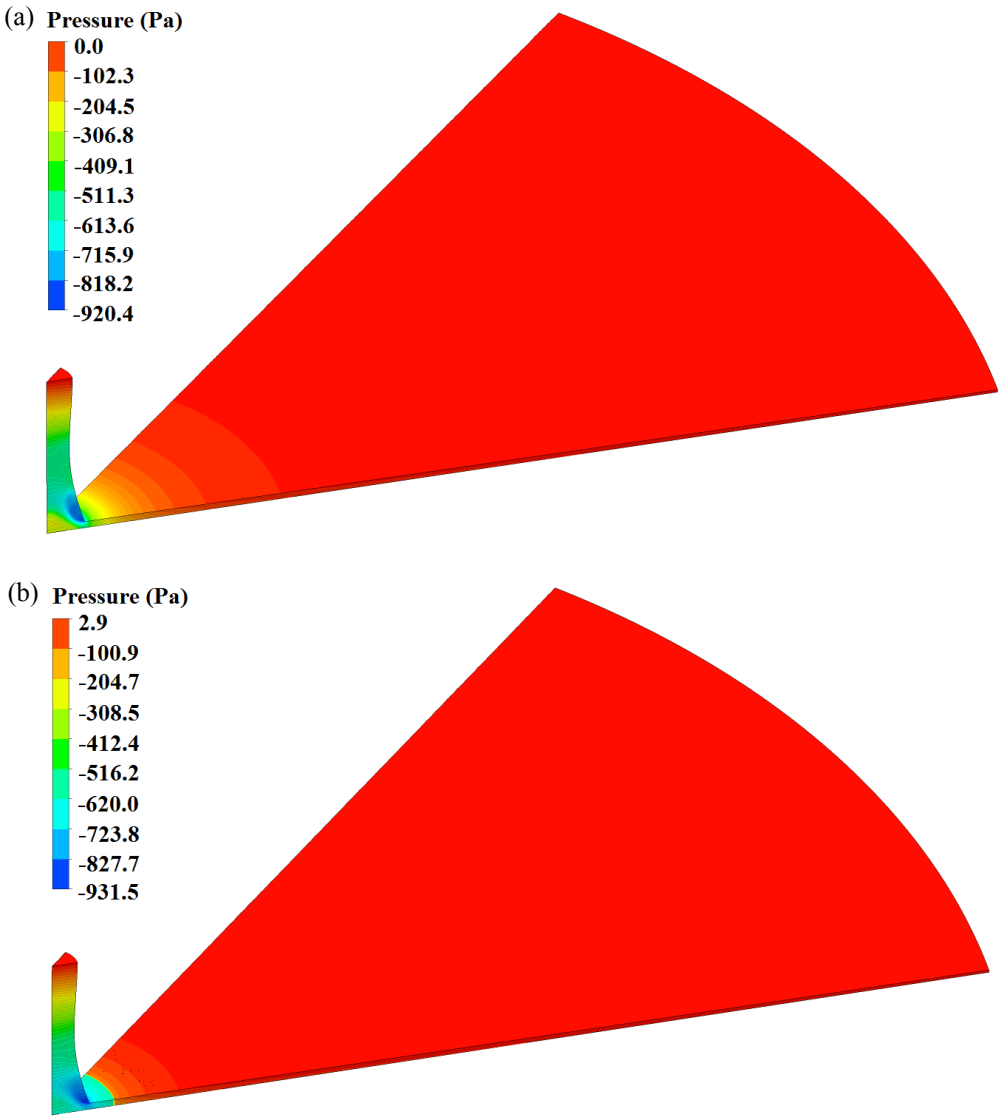

Fig. 3. Gauge pressure distribution at the boundaries of the computational domain for (a) no filter bank in the system, and (b) the filter bank present in the system.

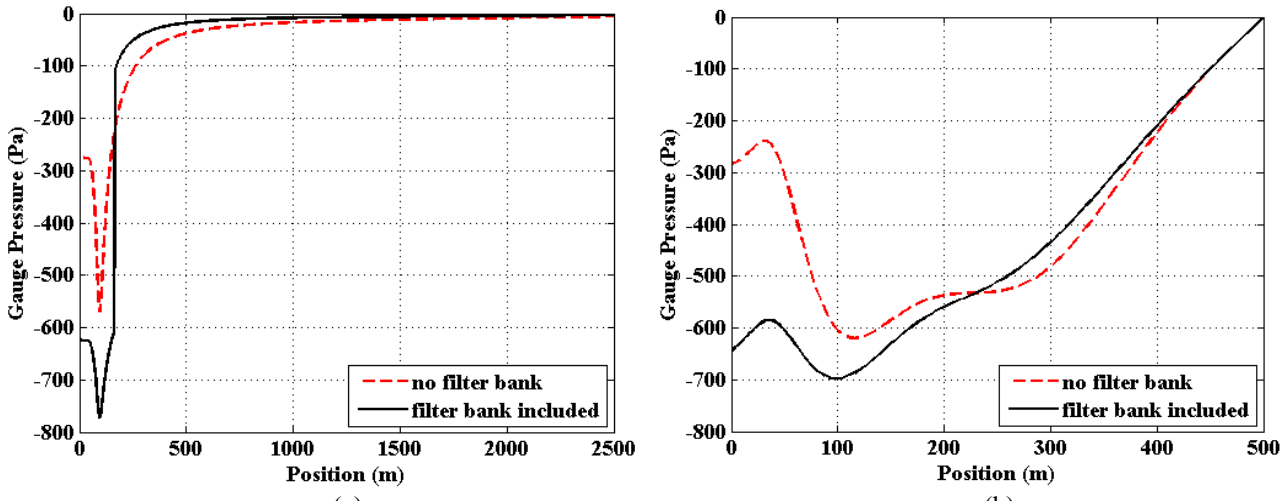

Fig. 4. Pressure distributions in SALSCS: (a) along the centerline of the collector, and (b) along the centerline of the chimney.

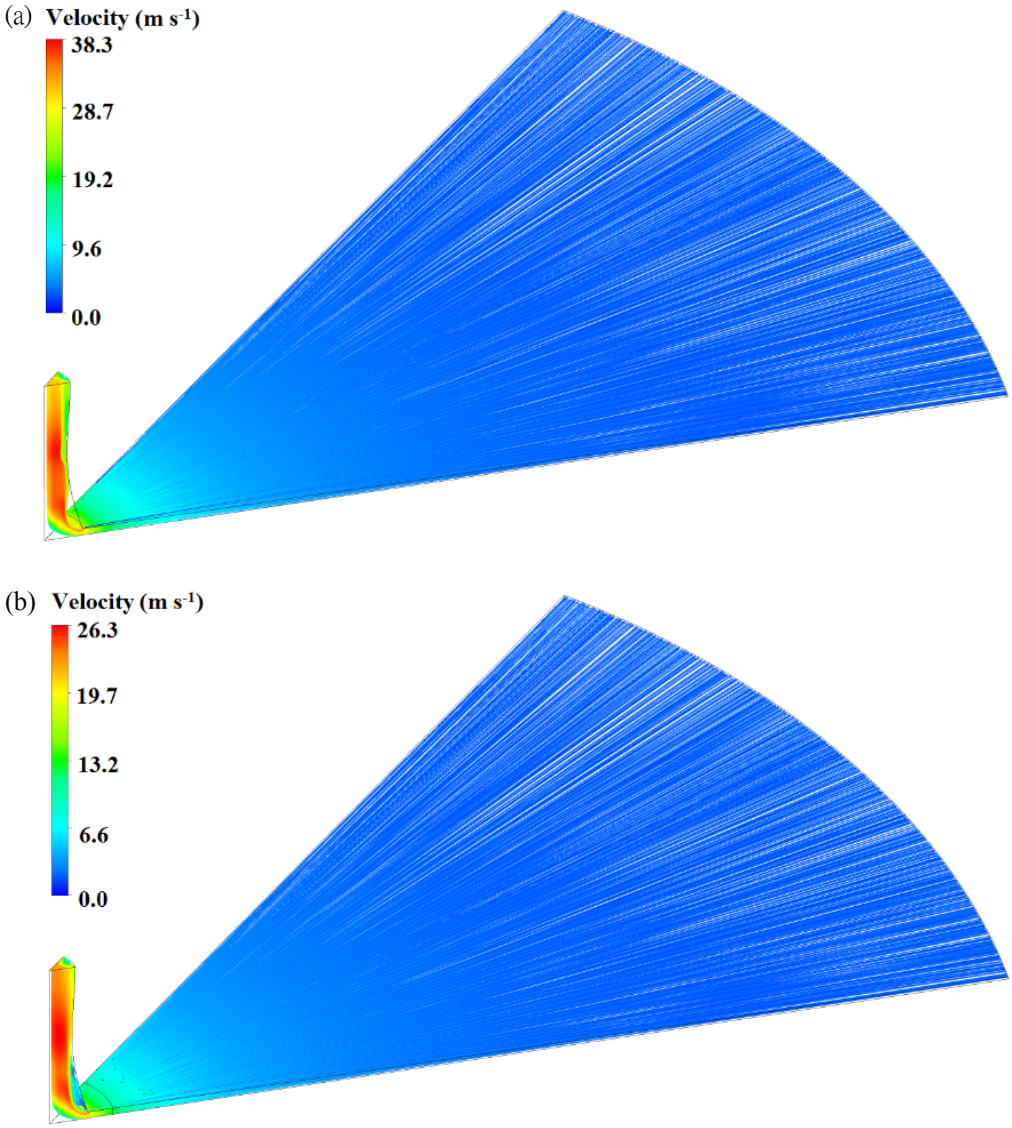

Fig. 5. Streamlines in SALCS for (a) no filter bank in the system, and (b) the filter bank present in the system.

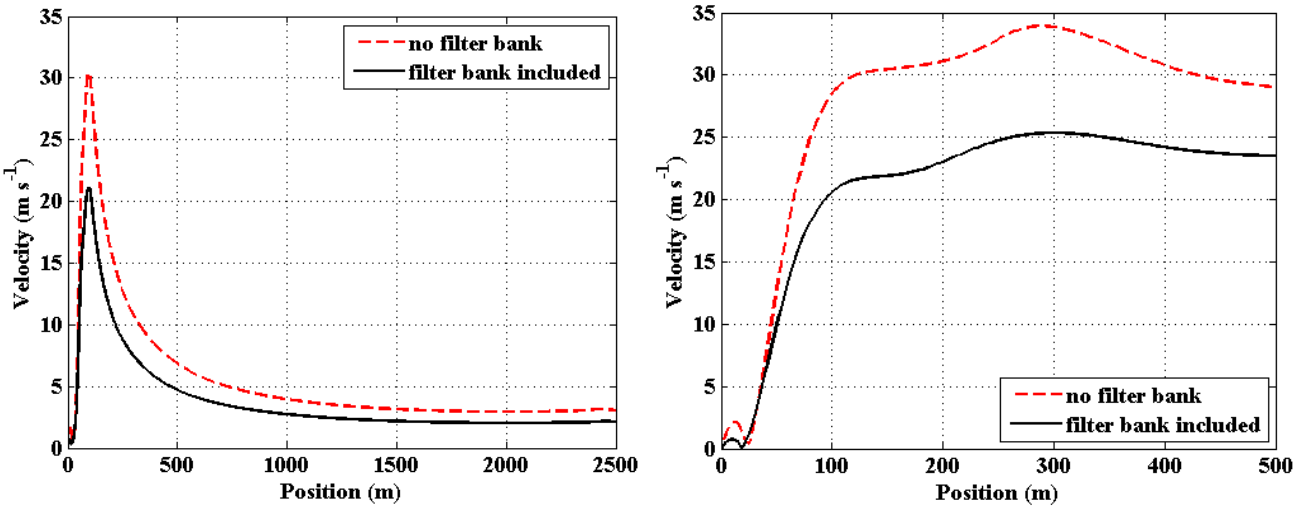

(a) (b)

Fig. 6. Velocity profiles of in SALSCS along the centerlines of (a) the collector, and (b) the chimney.

chimney with the narrowest cross-section area. Comparing the velocity profiles in Fig. 6, we know that the air flow speed is reduced with the filter bank implemented in SALSCS.

The local temperature values along the centerlines of the collector and the chimney are plotted in Figs. 7(a) and 7(b) respectively. According to Fig. 7(a), the temperature in the collector increases gradually from the inlet to the outlet of the collector. At the chimney bottom, there is a significant temperature increase by about 10 degrees, which is caused by the reduction of the local convective heat transfer rate with a relatively low air speed. Fig. 7(b) shows that the temperature in the chimney only decreases slightly from the chimney bottom to its outlet. This result can be referred to the adiabatic boundary condition applied at the chimney wall. In general, Fig. 7 indicates that a higher overall temperature in SALSCS is achieved if a filter bank is included in the system. As an explanation, the filter bank decreases the average velocity of the flow field and reduces the convective heat transfer effect in the whole system, leading to the increase of the overall system temperature.

The system volumetric flow rates are given in Table 3. Another factor named flow-rate/solar-collector-area ratio, γ, is also defined as follows, for evaluating the efficiency of the system:

$$\gamma = \frac{\dot{Q}}{A} \tag{13}$$

where $\dot{Q}$ is the volumetric flow rate and A is the area occupied by the solar collector. As indicated by Table 3, the filter bank reduces the flow rate of a SALSCS by 30.5%, and a system with the filter bank implemented can generate a volumetric flow rate of 2.64×10^5 m^3/s. Thus the system is able to clean 22.4 km^3 volume of air in 24 hours, and we believe that it can be more efficient with some optimizations in the future.

As a case study, a simple estimate is obtained for the city of Beijing, China. The municipality of Beijing has a total area of 16,801 km^2 including the suburban districts and rural counties. The urban area enclosed by the 6th Ring Road of the city, of approximately 300 km^2 and the volume of 750 km^3 (250 m height) is considered. A single SALSCS system can process about 3.04% of air in the considered volume for 24-hour operation. With multiple of the SALSCS systems employed, the approach proposed in this study is promising for urban air remediation in major cities around the world.

SUMMARY

In this paper, a Solar-Assisted Large-Scale Cleaning System (SALSCS) is presented for urban air remediation. By using numerical simulation as a tool, we have designed a SALSCS in ANSYS Fluent which is composed of a full-circle solar collector of 2500 m in diameter, a chimney of 500 m in height and a filter bank implemented vertically at a location in the collector. Based on the designed system geometry, the numerical simulation is conducted on two system configurations: a system with a filter bank and a system without a filter bank. According to our simulation results, the impacts of the filter bank on the system flow field has been analyzed and discussed. In general, with the

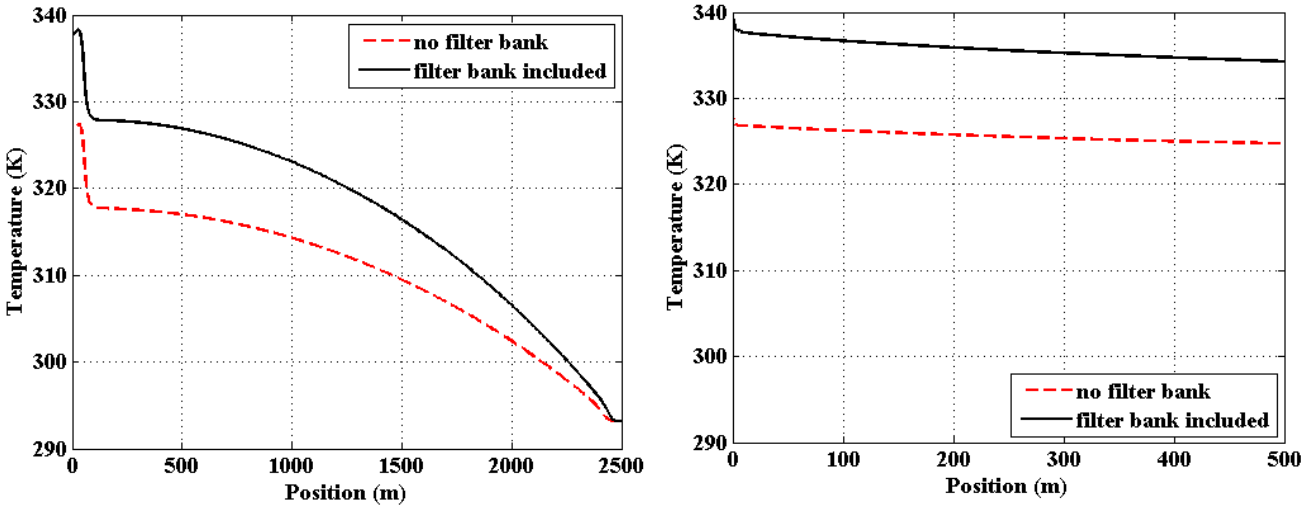

Fig. 7. Temperature profiles in SALSCS along the centerlines of (a) the collector, and (b) the chimney.

Table 3. Volumetric flow rates and flow-rate/green-house-area ratios of SALSCSs.

	System Volumetric Flow Rate (m^3/s)	Ratio of Flow-Rate/Solar-Collector-Area (m/s)
SALSCS without filter bank	3.80×10^5	0.0194
SALSCS with filter bank	2.64×10^5	0.0134

filter bank implemented, there is a decrease in system air flow velocity, and an increase for both the overall system pressure drop and temperature. In addition, our simulation also tells that a SALSCS of our design presented in this paper is able to generate a volumetric flow rate of 2.64×10^5 m^3/s, meaning that 22.4 km^3 of air can be cleaned by the system in 24 hours. We believe that SALSCS will be a promising method for solving air pollutions problems in urban areas worldwide.

NOMENCLATURE

A area occupied by the solar collector, m^2
C_μ, $C_{1\varepsilon}$, $C_{2\varepsilon}$, $C_{3\varepsilon}$ constants for turbulent model
c_p specific heat capacity, J/kg/K
D diameter, m
G_k turbulence kinetic energy generation due to the mean velocity gradients, J
g gravitational acceleration, m/s^2
K thermal conductivity, W/m/K
k turbulence kinetic energy, J/kg
L characteristic length, m
H height, m
h convective heat transfer coefficient, $W/m^2/K$
I turbulence intensity, %
n local coordinate normal to a surface
q'' heat flux from the ground surface, W/m^2
Pr_t turbulent Prandtl number for turbulent model
p pressure, Pa
$\dot{Q}$ volumetric flow rate, m^3/s
R radius, m
Ra Rayleigh number
T temperature, K
u velocity, m/s

Greek

α thermal diffusivity, m^2/s
β thermal expansion coefficient, K^{-1}
γ flow-rate/solar-collector-area ratio, m/s
Δp pressure drop across the filter bank, Pa
ε turbulence kinetic energy dissipation rate, W/kg
μ dynamic viscosity, kg/m/s
μ_t turbulent dynamic viscosity coefficient
ν kinematic viscosity, m^2/s
ρ air density, kg/m^3
σ_k, σ_ε turbulent Prandtl numbers for k and ε respectively

Subscripts

max maximum
min minimum
in inlet
out outlet
h hydraulic
∞ ambient
ch chimney
f filter bank
wr wall roughness
sc solar collector
t throat
i, j any direction of x, y and z

ACKNOWLEDGEMENTS

The authors wish to express our appreciation of the helpful discussion with Prof. Junji Cao of the Institute of Earth Environment of the Chinese Academy of Science (IEECAS), and with Prof. Wenquan Tao of the Xi'an Jiaotong University (XJTU), Xi'an, China. We would also like to thank the Minnesota Supercomputing Institute (MSI) for their support of computing resources.

REFERENCE

ANSYS (2012). ANSYS Fluent 14.5 Theory Guide. ANSYS, Inc.

Bernardes, M.A.S., Voß, A. and Weinrebe, G. (2003). Thermal and Technical Analysis of Solar Chimneys. *Sol. Energy* 75: 511–524.

Bernardes, M.A.S., Backström, T.W. and Kröger, D.G. (2007). Critical Evaluation of Heat Transfer Coefficients Applicable to Solar Chimney Power Plant Collectors. In *Proceedings of ISES Solar World Congress 2007*, Beijing, China, p. 1706–1713.

Bernstein, J.A., Alexis, N., Barnes, C., Bernstein, I.L., Nel, A., Peden, D., Diaz-Sanchez, D., Tarlo, S.M. and Williams, P.B. (2004). Health Effects of Air Pollution. *J. Allergy Clin. Immunol.* 114: 1116–1123.

Bilgen, E. and Rheault, J. (2005). Solar Chimney Power Plants for High Latitudes. *Sol. Energy* 79: 449–458.

Cao, F., Zhao, L. and Guo, L. (2011). Simulation of a Sloped Solar Chimney Power Plant in Lanzhou. *Energy Convers. Manage.* 52: 2360–2366.

Chen, Y., Ebenstein, A., Greenstone, M. and Li, H. (2013). Evidence on the Impact of Sustained Exposure to Air Pollution on Life Expectancy from China's Huai River Policy. *Proc. Nat. Acad. Sci. U.S.A.* 110: 12936–12941.

Cifuentes, L.A., Vega, J., Kopfer, K. and Lave L.B. (2000). Effect of the Fine Fraction of Particulate Matter versus the Coarse Mass and Other Pollutants on Daily Mortality in Santiago, Chile. *J. Air Waste Manage. Assoc.* 50: 1287–1298.

Dhahri, A. and Omri, A. (2013). A Review of Solar Chimney Power Generation Technology. *Int. J. Eng. Adv. Technol.* 2: 1–17.

Donaldson (2014). www.donaldson.com/en/index.html.

Fasel, H.F., Meng, F., Shams, E. and Gross, A. (2013). CFD Analysis for Solar Chimney Power Plants. *Sol. Energy* 98: 12–22.

Guo, P.H., Li, J.Y. and Wang, Y. (2014). Numerical Simulation of Solar Chimney Power Plant with Radiation Model. *Renewable Energy* 62: 24–30.

Guttikunda, S.K. and Calori, G. (2013). A GIS Based Emissions Inventory at 1 km ×1 km Spatial Resolution for Air Pollution Analysis in Delhi, India. *Atmos. Environ.* 67: 101–111.

Haaf, W., Friedrich, K., Mayr, G. and Schlaich, J. (1983). Solar Chimneys, Part I: Principle and Construction of the Pilot Plant in Manzanares. *Int. J. Sol. Energy* 2: 3–20.

Haaf, W. (1984). Solar Chimneys, Part II: Preliminary Test Results from the Manzanares Pilot Plant. *Int. J. Sol. Energy* 2: 141–161.

Itasca (2014). https://www.msi.umn.edu/hpc/itasca.

Krätzig, W.B., Gould, P.L. and Harte, R. (2011). In *Fifty Years of Progress for Shell and Spatial Structures*, Vol. 7, Mungan, I. and Abel, J.F. (Eds.), Multi-Science Publishing Co. Ltd, Essex, UK, p. 492.

Miller, K.A., Siscovick, D.S., Sheppard, L., Shepherd, K., Sullivan, J.H., Anderson, G.L. and Kaufman, J.D. (2007). Long-Term Exposure to Air Pollution and Incidence of Cardiovascular Events in Women. *New Engl. J. Med.* 356: 447–458.

Ming, T., Liu, W. and Xu, G. (2006). Analytical and Numerical Investigation of the Solar Chimney Power Plant System. *Int. J. Energy Res.* 30: 861–873.

Ming, T., Liu, W., Pan, Y. and Xu, G. (2008a). Numerical Analysis of Flow and Heat Transfer Characteristics in Solar Chimney Power Plants with Energy Storage Layer. *Energy Convers. Manage.* 49: 2872–2879.

Ming, T., Liu, W., Xu, G., Xiong, Y., Guan, X. and Pan, Y. (2008b). Numerical Simulation of the Solar Chimney Power Plant Systems Coupled with Turbine. *Renewable Energy* 33: 897–905.

Ming, T., Wang, X., Richter, R.K., Liu, W., Wu, T. and Pan, Y. (2012). Numerical Analysis on the Influence of Ambient Crosswind on the Performance of Solar Updraft Power Plant System. *Renewable Sustainable Energy Rev.* 16: 5567–5583.

Ming, T., Richter, R.K., Meng, F., Pan, Y. and Liu, W. (2013). Chimney Shape Numerical Study for Solar Chimney Power Generating Systems. *Int. J. Energy Res.* 37: 310–322.

Monks, P.S., Granier, C., Fuzzi, S., Stohl, A., Williams, M.L., Akimoto, H., Amann, M., Baklanov, A., Baltensperger, U., Bey, I., Blake, N., Blake, R.S., Carslaw, K., Cooper, O.R., Dentener, F., Fowler, D., Fragkou, E., Frost, G.J., Generoso, S., Ginoux, P., Grewe, V., Guenther, A., Hansson, H.C., Henne, S., Hjorth, J., Hofzumahaus, A., Huntrieser, H., Isaksen, I.S.A., Jenkin, M.E., Kaiser, J., Kanakidou, M., Klimont, Z., Kulmala, M., Laj, P., Lawrence, M.G., Lee, J.D., Liousse, C., Maione, M., McFiggans, G., Metzger, A., Mieville, A., Moussiopoulos, N., Orlando, J.J., O'Dowd, C.D., Palmer, P.I., Parrish, D.D., Petzold, A., Platt, U., Pöschl, U., Prévôt, A.S.H., Reeves, C.E., Reimann, S., Rudich, Y., Sellegri, K., Steinbrecher, R., Simpson, D., Brink, H., Theloke, J., Werf, G.R., Vautard, R., Vestreng, V., Vlachokostas, Ch. and Glasow, R. (2009). Atmospheric Composition Change – Global and Regional Air Quality. *Atmos. Environ.* 43: 5268–5350.

Panse, S.V., Jadhav, A.S., Gudekar, A.S. and Joshi, J.B. (2011). Inclined Solar Chimney for Power Production. *Energy Convers. Manage.* 52: 3096–3102.

Pastohr, H., Kornadt, O. and Gürlebeck, K. (2004). Numerical and Analytical Calculations of the Temperature and Flow Field in the Upwind Power Plant. *Int. J. Energy Res.* 28: 495–510.

Pasumarthi, N. and Sherif, S.A. (1998a). Experimental and Theoretical Performance of a Demonstration Solar Chimney Model – Part I: Mathematical Model Development. *Int. J. Energy Res.* 22: 277–288.

Pasumarthi, N. and Sherif, S.A. (1998b). Experimental and Theoretical Performance of a Demonstration Solar Chimney Model – Part II: Experimental and Theoretical Results and Economic Analysis. *Int. J. Energy Res.* 22: 443–461.

Pope III, C.A. and Dockery D.W. (2006). Health Effects of Fine Particulate Air Pollution: Lines that Connect. *J. Air Waste Manage. Assoc.* 56: 709–742.

Pope III, C.A., Ezzati, M. and Dockery, D.W. (2009). Fine-Particulate Air Pollution and Life Expectancy in the United States. *New Engl. J. Med.* 360: 376–386.

Pöschl, U. (2005). Atmospheric Aerosols: Composition, Transformation, Climate and Health Effects. *Angew. Chem. Int. Ed.* 44: 7520–7540.

Pui, D.Y.H., Chen, S.C. and Zuo, Z. (2014). $PM_{2.5}$ in China: Measurements, Sources, Visibility and Health Effects, and Mitigation. *Particuology* 13: 1–26.

Ramanathan, V. and Feng, Y. (2009). Air Pollution, Greenhouse Gases and Climate Change: Global and Regional Perspectives. *Atmos. Environ.* 43: 37–50.

Sangi, R., Amidpour, M. and Hosseinizadeh, B. (2011). Modeling and Numerical Simulation of Solar Chimney Power Plants. *Sol. Energy* 85: 829–838.

Schlaich, J., Bergermann, R., Schiel, W. and Weinrebe, G. (2005). Design of Commercial Solar Updraft Tower Systems – Utilization of Solar Induced Convective Flows for Power Generation. *J. Sol. Energy Eng.* 127: 117–124.

Schwartz, J., Dockery, D.W. and Neas, L.M. (1996). Is Daily Mortality Associated Specifically with Fine Particles? *J. Air Waste Manage. Assoc.* 46: 927–939.

Seaton, A., MacNee, W., Donaldson, K. and Godden, D. (1995). Particulate Air Pollution and Acute Health Effects. *Lancet* 345: 176–178.

Shah, A.S.V., Langrish, J.P., Nair, H., McAllister, D.A., Hunter, A.L., Donaldson, K., Newby, D.E. and Mills, N.L. (2013). Global Association of Air Pollution and Heart Failure: A Systematic Review and Meta-Analysis. *Lancet* 382: 1039–1048.

Spiegel, E.A. and Veronis, G. (1960). On the Boussinesq Approximation for a Compressible Fluid. *Astrophys. J.* 131: 442–447.

Zhou, X., Yang, J., Xiao, B. and Hou, G. (2007). Simulation of a Pilot Solar Chimney Thermal Power Generating Equipment. *Renewable Energy* 32: 1637–1644.

Zhou, X., Wang, F. and Ochieng, R.M. (2010). A Review of Solar Chimney Power Technology. *Renewable Sustainable Energy Rev.* 14: 2315–2338.

Received for review, October 12, 2014
Revised, October 12, 2014
Accepted, November 15, 2014